

Article

# Effect of SrTiO<sub>3</sub> Nanoparticles in Conductive Polymer on the Thermoelectric Performance for Efficient Thermoelectrics

Dabin Park, Hyun Ju and Jooheon Kim \* 

School of Chemical Engineering & Materials Science, Chung-Ang University, Seoul 06974, Korea; dragoo@naver.com (D.P.); mohani@cau.ac.kr (H.J.)

\* Correspondence: jooheonkim@cau.ac.kr

Received: 18 November 2019; Accepted: 27 March 2020; Published: 1 April 2020



**Abstract:** We present hybrid organic inorganic materials, namely, SrTiO<sub>3</sub>/polyaniline (PANI) composites, with high thermoelectric performance; samples with various SrTiO<sub>3</sub> contents (10, 20, 30, and 50 wt.%) were prepared. The PANI component was obtained through the polymerization of aniline monomers, followed by camphorsulfonic acid-doping to enhance its electrical conductivity. SrTiO<sub>3</sub>, with a high Seebeck coefficient, was used as the N-type inorganic component; it was synthesized via a one-pot solvothermal method and, then, dispersed into the conductive PANI matrix. The SrTiO<sub>3</sub> content influenced the Seebeck coefficient and electrical conductivity of the resulting composites. The variations in the thermoelectric properties of the SrTiO<sub>3</sub>/PANI composites consequently changed their power factor; at room temperature, the highest value was ~49.6 μW·m/K<sup>2</sup>, which is 17 times larger than that of pure PANI.

**Keywords:** thermoelectric; polyaniline; strontium titanate; nanostructure

## 1. Introduction

Thermoelectric (TE) power generation is a core technology for renewable energy harvesting and greenhouse gas reduction because of the potential energy conversion between thermal and electrical energies [1–9]. The efficiency of TE materials can be evaluated by the dimensionless figure of merit,  $ZT = S^2 \cdot \sigma \cdot T / \kappa$ , where  $S$ ,  $\sigma$ ,  $T$ , and  $\kappa$  are, respectively, the Seebeck coefficient, the electrical conductivity, the absolute temperature, and the total thermal conductivity. The previous studies generally focused on inorganic TE materials such as Te-based compounds (Bi<sub>2</sub>Te<sub>3</sub>, Ag<sub>2</sub>Te, and Cu<sub>2</sub>Te) [10–12], Se alloys (SnSe, Cu<sub>2</sub>Se) [13–15], and conducting oxides (NaCo<sub>2</sub>O<sub>4</sub>, CaMnO<sub>3</sub>) [16,17]; however, these materials are typically expensive and brittle, which prevents their application in large areas. Thus, polymer-based TE materials have recently been widely used for energy harvesting due to their unique advantages, i.e., low cost, low processing temperature, and mechanical flexibility. In this regard, we have developed high-efficiency metal polymer TE devices [18–20].

The  $ZT$  can be simply achieved by a low thermal conductivity or with a high power factor ( $PF = S^2 \cdot \sigma$ ). Currently, conductive polymers such as poly(3,4-ethylenedioxythiophene)-poly(4-styrenesulfonate) (PEDOT:PSS), polypyrrole, and polythiophene are being used as TE base materials because of their outstanding thermoelectric properties [21–23]. Ju et al. enhanced the thermoelectric properties of a conductive PEDOT:PSS matrix by incorporation SnSe nanosheets [24]. SnSe nanosheet/PEDOT:PSS composites have exhibited also enhanced  $ZT$  (0.32) at room temperature, which is ~6 times larger than that of pristine PEDOT:PSS. Polyaniline (PANI) is another promising conductive polymer due to its unique characteristics, namely, high  $\sigma$ , and low  $\kappa$  [25–28]; Anno et al. prepared camphorsulfonic acid (CSA)-doped PANI [29], observing an increased  $PF$  of ~0.02 μWm/K<sup>2</sup>. Wang et al. observed a  $\sigma$  of

~65 S/cm for pure PANI and prepared a PANI/Te nanorod composite via a solution mixing method, achieving high  $PF$  (~80  $\mu\text{Wm}/\text{K}^2$ ) at high temperature [30].

Perovskite strontium titanate and its composites are recently being widely used as N-type materials due to their high  $S$  and chemical stability. In particular, at room temperature,  $\text{SrTiO}_3$  has an outstanding  $S$  (~400  $\mu\text{V}/\text{K}$ ) [27] compared to other extensively used N-type materials such as  $\text{Bi}_2\text{Te}_3$ ,  $\text{Sb}_2\text{Te}_3$ , and  $\text{Ag}_2\text{Te}$  [31–34].

In this study, we suggest a strategy to increase the thermoelectric performance by fabrication of hybrid polymer-based TE composites, namely,  $\text{SrTiO}_3/\text{PANI}$  composites. The PANI matrix was synthesized through the polymerization of aniline monomers, followed by the doping with CSA to enhance its  $\sigma$ .  $\text{SrTiO}_3$  was prepared via a one-pot solvothermal method by using Sr and Ti precursor solutions. Then, different  $\text{SrTiO}_3$  contents were incorporated into the PANI matrix to obtain hybrid organic-inorganic TE composites, whose thermoelectric properties ( $S$ ,  $\sigma$ , and  $PF$ ) were successively analyzed. We expected that the  $\text{SrTiO}_3$  nanoparticles were randomly dispersed within the PANI matrix, providing a highly efficient thermoelectric performance.

## 2. Experimental

### 2.1. Materials

Sodium hydroxide (NaOH, 98%), ethanol ( $\text{C}_2\text{H}_5\text{OH}$ , 94%) and hydrochloric acid (HCl, 99%) were purchased from Sigma Aldrich (St. Louis, MO, USA). Strontium nitrate ( $\text{Sr}(\text{NO}_3)_2$ , 98%), titanium tetraisopropoxide [ $(\text{CH}_3)_2\text{CHO}$ ] $_4\text{Ti}$  (TTIP, 98%), ammonium persulfate (APS, 98%), aniline (99%), and D(+)-camphorsulfonic acid (CSA, 98%) were provided by Daejung Chemicals & Metals Co. (Seoul, Korea). All chemicals were used without further purification.

### 2.2. Preparation of PANI

A PANI powder was produced via the chemical polymerization of aniline monomers by using HCl as the dopant and APS as the oxidant. According to the typical synthetic procedure, the monomers (0.05 g) were dispersed in 25 mL of 1M HCl and sonicated the mixture at room temperature. Then, another 1 M HCl solution (1 mL) containing 0.01 g of APS was slowly added to this colloidal solution, followed by steady stirring for 12 h to obtain an aniline/HCL suspension. Next, the polymerization reaction was carried out at 0 °C under stirring for 6 h in an ice bath. The products were filtered and sequentially washed with 1 M HCl, deionized (DI) water, and ethanol, followed by CSA doping to improve the PANI electrical conductivity. The resulting PANI powder was further doped with CSA at a mole ratio of 1:0.6 through a solid-state reaction.

### 2.3. Synthesis of $\text{SrTiO}_3$

First,  $\text{Sr}(\text{NO}_3)_2$  (1.9 g) and TTIP (2.55 g) were dissolved in DI water (30 mL) and ethanol (180 mL), respectively. The Sr precursor solution was then slowly added to the Ti one, which was subsequently heated and stirred at 50 °C for 30 min. Next, a 0.2 M NaOH aqueous solution (10 mL) was added to the mixture, followed by stirring for another 30 min. Afterwards, the as-obtained solution was poured into a Teflon-lined autoclave and heated at 140 °C for 24 h. The resulting product ( $\text{SrTiO}_3$ ) was filtered, washed repeatedly, and loaded into a quartz ampoule that was successively sealed with a flame at 350 °C for 30 min.

### 2.4. Preparation of $\text{SrTiO}_3/\text{PANI}$ Composites

A quantity of 0.1 g of the CSA-doped PANI and various amounts (10, 20, 30, and 50 wt.%) of  $\text{SrTiO}_3$  were dissolved in m-cresol. These mixtures were stirred for 6 h and filtered twice with DI water and ethanol. Finally, the as-prepared  $\text{SrTiO}_3/\text{PANI}$  composites were dried in a vacuum oven, ground into fine powders, and hot-pressed at 80 °C for 10 min under 50 MPa.

### 2.5. Characterization of the SrTiO<sub>3</sub>/PANI Composites

The morphology of the samples was examined with a field emission scanning electron microscopy (FE-SEM) system (SIGMA, Oberkochen, German), while their element maps were obtained with an energy dispersive X-ray spectroscopy (EDS) instrument (NORAN system 7, Thermo scientific, Seoul, Korea). An X-ray diffraction (XRD) analyzer (New D8-Advance, Bruker-AXS) with Cu K $\alpha$  radiation (0.154056 nm) was used to identify the crystal phase of the composites; the XRD patterns were acquired in a  $2\theta$  range of 20 to 80° at a scan rate of 1°/s. The binding energy peaks were analyzed by using an X-ray photoelectron spectroscopy (XPS) system (Thermo U.K. K-alpha, Seoul, Korea) with Al K $\alpha$  radiation (1486.6 eV).

Disc-shaped samples with a 12.7 mm diameter were prepared to determine  $\sigma$  and  $S$ . The electrical conductivity was derived by using a Keithley 2400 source meter and the four-point probe method; the thickness of the samples was measured with a digital micrometer. The Seebeck coefficient was estimated with homemade equipment consisting of a pair of voltmeters and thermocouples. Five SrTiO<sub>3</sub>/PANI samples were prepared for the reproducibility of the experiments and the average values are reported here.

## 3. Results and Discussion

In the formation of SrTiO<sub>3</sub> via the one-pot solvothermal method, NaOH plays a key role as follows. The high OH<sup>-</sup> concentration provided by the NaOH solution promotes the hydrolysis of TTIP, yielding negatively charged Ti sol that successively reacts with the Sr cations from the Sr precursor, finally forming SrTiO<sub>3</sub> [31].

The XRD patterns of synthesized SrTiO<sub>3</sub> (Figure 1a) showed diffraction peaks at 32.4°, 39.9°, 46.5°, 57.8°, 67.8°, and 77.2°. that were attributed to, respectively, the (100), (111), (200), (211), and (220) planes of perovskite SrTiO<sub>3</sub> (JCPDS no. 35-0734), indicating the formation of pristine SrTiO<sub>3</sub> with a well-defined cubic by structure [35,36].

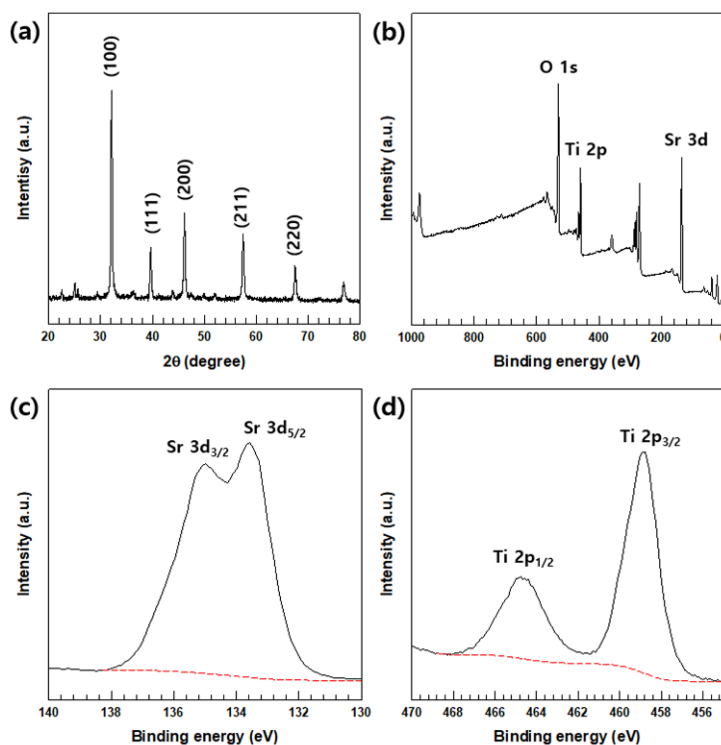


**Figure 1.** (a) XRD patterns, along with the XPS (b) survey and high-resolution (c) Sr 3d and (d) Ti 2p spectra, of the synthesized SrTiO<sub>3</sub> nanoparticles.

The successful synthesis and chemical composition of SrTiO<sub>3</sub> was then confirmed by the XPS results. In the XPS survey spectrum (Figure 1b), the Sr 3d and Ti 2p peaks were observed. The high-resolution Sr 3d spectrum (Figure 1c) showed peaks at ~132 and ~134 eV that correspond to the Sr 3d<sub>5/2</sub> and 3d<sub>3/2</sub> binding energies, respectively, of pristine SrTiO<sub>3</sub>, suggesting its existence in the Sr<sup>2+</sup> state. Ti existed as Ti<sup>4+</sup>, as revealed by the two separate peaks at ~463 and ~458 eV, corresponding to Ti 2p<sub>1/2</sub> and Ti 2p<sub>3/2</sub>, respectively (Figure 1d) [37].

The FE-SEM analysis clearly showed the nano-sized (~50–100 nm) grains of the synthesized SrTiO<sub>3</sub> (Figure 2a,b). Furthermore, the corresponding Sr and Ti maps (Figure 2c,d) confirmed its unary composition.

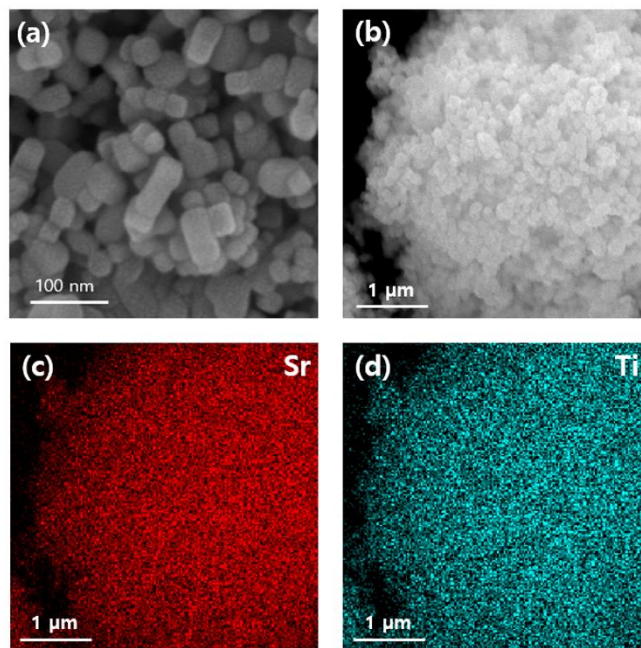


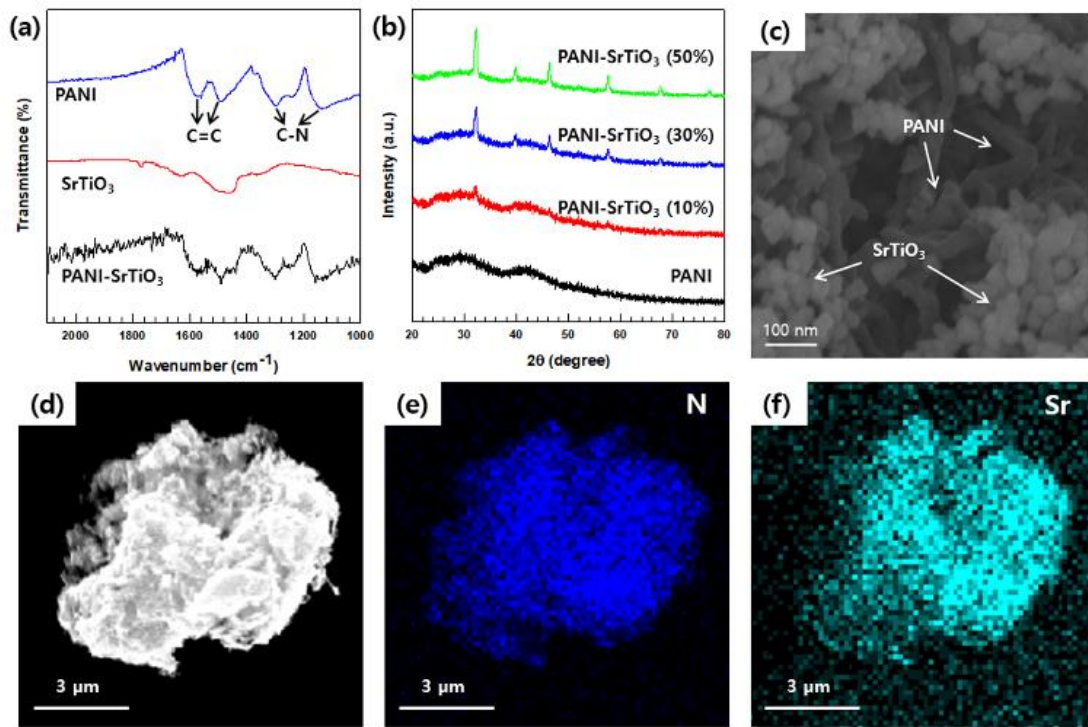
**Figure 2.** (a,b) Field emission scanning electron microscopy (FE-SEM) and energy dispersive X-ray spectroscopy (EDS) images of SrTiO<sub>3</sub>. (c,d) Elemental maps of (b), obtained via energy dispersive X-ray spectroscopy.

The FT-IR spectra (Figure 3a) exhibited two bands at ~1580 and ~1450 cm<sup>-1</sup> and another two at ~1300 and ~1140 cm<sup>-1</sup>; these signal pairs were attributed to the C=C vibration and the C–N structure, respectively, of the quinoid and benzoid rings in PANI [38,39]. The successful preparation of the SrTiO<sub>3</sub>/PANI composites was then confirmed by their XRD patterns (Figure 3b), which showed that the SrTiO<sub>3</sub> peaks systematically gained intensity as the SrTiO<sub>3</sub> content increased. These peaks demonstrate the good dispersion of SrTiO<sub>3</sub> and PANI in the sample composite matrix. The FE-SEM observation of the SrTiO<sub>3</sub> (30 wt.%) /PANI sample (Figure 3c) further confirmed the uniform dispersion of these two components. Their random dispersion was also demonstrated, along with the successful synthesis of SrTiO<sub>3</sub>/PANI, via the EDS elemental mapping (Figure 3d–f).

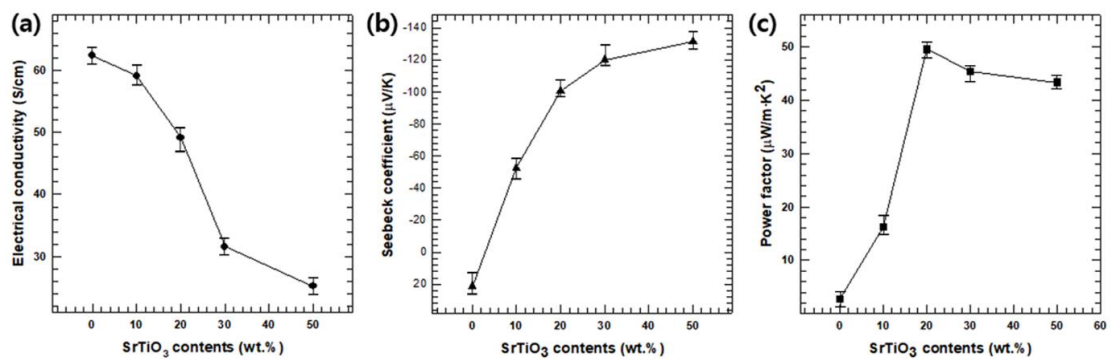
For the measurements of the TE properties, the PANI and SrTiO<sub>3</sub>/PANI disks were loaded into a Fe mold and pressed at 200 °C under 50 MPa for 10 min.

Figure 4a compared electrical conductivities at room temperature of the various SrTiO<sub>3</sub> /PANI samples and pristine PANI (i.e., 0 wt.%). The pristine PANI sample exhibited a  $\sigma$  value of 62.4 S/cm, which is consistent with previous results [26]. As regards the composite sample,  $\sigma$  decreased with the increase in the SrTiO<sub>3</sub> contents; this was due to its relatively lower  $\sigma$  of SrTiO<sub>3</sub> compared to that of PANI [26]. This trend can be explained by the relation of  $\sigma$  with the charge carrier mobility ( $\mu$ ) and concentration ( $n$ ):  $\sigma = n \cdot e \cdot \mu$ , where  $e$  is the electron charge. According to this relation,  $\sigma$  is directly

proportional to  $n$  and  $\mu$ , whose values are given in Figure S1. For the SrTiO<sub>3</sub>/PANI samples,  $n$  decreased when increasing the SrTiO<sub>3</sub> content, resulting in the above-mentioned  $\sigma$  reduction.



**Figure 3.** (a) FT-IR spectra of the synthesized polyaniline (PANI), SrTiO<sub>3</sub>, and SrTiO<sub>3</sub> (30 wt.%) /PANI composite. (b) X-ray diffraction (XRD) patterns of pure PANI and the SrTiO<sub>3</sub>/PANI composites with different contents SrTiO<sub>3</sub>. (c) FE-SEM images and (d–f) EDS maps of SrTiO<sub>3</sub>(30 wt.%) /PANI.



**Figure 4.** (a) Electrical conductivity, (b) Seebeck coefficient, and (c) Power factor of the SrTiO<sub>3</sub>/PANI composites as functions of the SrTiO<sub>3</sub> content.

The pristine PANI sample exhibited a positive  $S$  (Figure 4b), confirming its P-type semiconducting behavior. On the other hand, the SrTiO<sub>3</sub>/PANI composites showed negative  $S$  values due to the N-type semiconducting behavior of SrTiO<sub>3</sub>; furthermore, the absolute  $S$  value increased along with the SrTiO<sub>3</sub> content because of the high  $S$  of SrTiO<sub>3</sub> at room temperature ( $\sim -300$   $\mu\text{V/K}$ ) [40]. The Seebeck coefficient of a material is generally inversely proportional to  $\mu$  and this trend is described by the following model [41,42]:

$$S = \frac{8 \cdot \pi^2 \cdot k_B^2}{3 \cdot e \cdot h^2} \cdot m^* \cdot T \cdot \left(\frac{\pi}{3 \cdot n}\right)^{\frac{2}{3}} \quad (1)$$

where  $k_B$  is the Boltzmann constant,  $h$ , is the Planck constant, and  $m^*$  is the effective mass of the charge carrier.

When increasing the absolute  $S$  and decreasing  $\sigma$ , at room temperature, the SrTiO<sub>3</sub>(20 wt.%)/PANI sample exhibited the largest  $PF$ , i.e.,  $\sim 29.6 \mu\text{W}\cdot\text{m}/\text{K}^2$ , which is 17 times larger than that of pristine PANI.

In this study, we prepared SrTiO<sub>3</sub>/PANI composites and evaluated their thermoelectric properties. With increasing the SrTiO<sub>3</sub> content,  $S$  accordingly increased while  $\sigma$  decreased. Therefore, the maximum  $PF$  was obtained for the composite. These experimental results can provide a strategy for achieving highly efficient TE materials.

#### 4. Conclusions

We fabricate SrTiO<sub>3</sub>/PANI composites with various SrTiO<sub>3</sub> contents and analyzed their thermoelectric properties. The purpose was to fabricate PANI-based materials with high thermoelectric efficiency. The PANI and SrTiO<sub>3</sub> components were synthesized via, respectively, the polymerization of aniline monomers and a one-pot solvothermal method with Sr and Ti precursor solutions; NaOH was crucial in the SrTiO<sub>3</sub> nanoparticle growth. The morphology and nanostructure of the composites were characterized through XRD, XPS, FT-IR, FE-SEM, and EDS analyses. Upon increasing the SrTiO<sub>3</sub> content,  $\sigma$  decreased because of the low  $\sigma$  of SrTiO<sub>3</sub>, while  $S$  increased. Due to these two trends, at room temperature, the sample with 20 wt.% SrTiO<sub>3</sub> exhibited the maximum power factor of  $\sim 49.6 \mu\text{W}\cdot\text{m}/\text{K}^2$ , which is  $\sim 17$  times larger than that of pure PANI. The results of this study demonstrate that the combination of SrTiO<sub>3</sub> with PANI as the organic polymer is a successful strategy to fabricate outstanding organic–inorganic TE materials.

**Supplementary Materials:** The following are available online at <http://www.mdpi.com/2073-4360/12/4/777/s1>, Figure S1: (a) carrier concentration, and (b) Carrier mobility of PANI–SrTiO<sub>3</sub> composites with various SrTiO<sub>3</sub> contents at room temperature, Figure S2: (a) FE-SEM images of (a). pristine PANI, (b) pristine SrTiO<sub>3</sub>, and (c) PANI–SrTiO<sub>3</sub> composites, Table S1. Seebeck coefficient, electrical conductivity, carrier concentration, and carrier mobility of PANI–SrTiO<sub>3</sub> composites at room temperature.

**Author Contributions:** Conceptualization, J.K.; Data curation, H.J.; Formal analysis, D.P. All authors have read and agreed to the published version of the manuscript.

**Funding:** This research received no external funding.

**Acknowledgments:** This work was supported by the Human Resources Development (No. 20184030202070) of the Korea Institute of Energy Technology Evaluation and Planning (KETEP) grant funded by the Korea government Ministry of Trade, Industry and Energy.

**Conflicts of Interest:** The authors declare no conflict of interest

#### References

1. Lin, L.; Wang, M.; Peng, X.; Lissek, E.N.; Mao, Z.; Scarabelli, L.; Adkins, E.; Coskun, S.; Unalan, H.E.; Korgel, B.A.; et al. Opto-thermoelectric nanotweezers. *Nat. Photonics* **2018**, *12*, 195–201. [[CrossRef](#)] [[PubMed](#)]
2. Yang, L.; Chen, Z.-G.; Dargusch, M.S.; Zou, J. High performance thermoelectric Materials: Progress and their applications. *Adv. Energy Mater.* **2018**, *8*, 1701797. [[CrossRef](#)]
3. Blackburn, J.L.; Ferguson, A.J.; Cho, C.; Grunlan, J.C. Carbon-nanotube-based thermoelectric materials and devices. *Adv. Mater.* **2018**, *30*, 1704386. [[CrossRef](#)] [[PubMed](#)]
4. Yao, H.; Fan, Z.; Cheng, H.; Guan, X.; Wang, C.; Sun, K.; Ouyang, J. Recent development of thermoelectric polymers and composites. *Macromol. Rapid Commun.* **2018**, *39*, 1700727. [[CrossRef](#)] [[PubMed](#)]
5. Snyder, G.J.; Toberer, E.S. Complex thermoelectric materials. *Nat. Mater.* **2008**, *7*, 105–114. [[CrossRef](#)]
6. Zebarjadi, M.; Esfarjani, K.; Dresselhaus, M.; Ren, Z.; Chen, G. Perspectives on thermoelectrics: From fundamentals to device applications. *Energy Environ. Sci.* **2012**, *5*, 5147–5162. [[CrossRef](#)]
7. Zhang, Q.; Sun, Y.; Xu, W.; Zhu, D. Organic thermoelectric materials: Emerging green energy materials converting heat to electricity directly and efficiently. *Adv. Mater.* **2014**, *26*, 6829–6851. [[CrossRef](#)]
8. Biswas, K.; He, J.; Blum, I.D.; Wu, C.-I.; Hogan, T.P.; Seidman, D.N.; Dravid, V.P.; Kanatzidis, M.G. High-performance bulk thermoelectrics with all-scale hierarchical architectures. *Nature* **2012**, *489*, 414. [[CrossRef](#)]
9. Liu, W.; Jie, Q.; Kim, H.S.; Ren, Z. Current progress and future challenges in thermoelectric power generation: From materials to devices. *Acta Mater.* **2015**, *87*, 357–376. [[CrossRef](#)]

10. Fang, H.; Yang, H.; Wu, Y. Thermoelectric properties of silver telluride–bismuth telluride nanowire heterostructure synthesized by site-selective conversion. *Chem. Mater.* **2014**, *26*, 3322–3327. [[CrossRef](#)]
11. Zhao, W.; Tan, H.T.; Tan, L.P.; Fan, S.; Hng, H.H.; Boey, Y.C.F.; Beloborodov, I.; Yan, Q. N-type carbon nanotubes/silver telluride nanohybrid buckypaper with a high-thermoelectric figure of merit. *ACS Appl. Mater. Interfaces* **2014**, *6*, 4940–4946. [[CrossRef](#)] [[PubMed](#)]
12. Park, D.; Ju, H.; Oh, T.; Kim, J. Facile fabrication of one-dimensional Te/Cu<sub>2</sub>Te nanorod composites with improved thermoelectric power factor and low thermal conductivity. *Sci. Rep.* **2018**, *8*, 18082. [[CrossRef](#)]
13. Ju, H.; Park, D.; Kim, J. Solution-processable flexible thermoelectric composite films based on conductive polymer/SnSe<sub>0.8</sub>S<sub>0.2</sub> nanosheets/carbon nanotubes for wearable electronic applications. *J. Mater. Chem. A* **2018**, *6*, 5627–5634. [[CrossRef](#)]
14. Ju, H.; Kim, M.; Park, D.; Kim, J. A strategy for low thermal conductivity and enhanced thermoelectric performance in SnSe: Porous SnSe<sub>1-x</sub>S<sub>x</sub> nanosheets. *Chem. Mater.* **2017**, *29*, 3228–3236. [[CrossRef](#)]
15. Yang, L.; Chen, Z.-G.; Han, G.; Hong, M.; Zou, Y.; Zou, J. High-performance thermoelectric Cu<sub>2</sub>Se nanoplates through nanostructure engineering. *Nano Energy* **2015**, *16*, 367–374. [[CrossRef](#)]
16. Terasaki, I. Transport properties and electronic states of the thermoelectric oxide NaCo<sub>2</sub>O<sub>4</sub>. *Physica B* **2003**, *328*, 63–67. [[CrossRef](#)]
17. Wang, Y.; Sui, Y.; Fan, H.; Wang, X.; Su, Y.; Su, W.; Liu, X. High temperature thermoelectric response of electron-doped CaMnO<sub>3</sub>. *Chem. Mater.* **2009**, *21*, 4653–4660. [[CrossRef](#)]
18. Ju, H.; Park, D.; Kim, K.; Kim, J. Exfoliated Sn–Se–Te based nanosheets and their flexible thermoelectric composites with poly (3, 4-ethylenedioxythiophene): Poly (styrenesulfonate) fabricated by solution processing. *Org. Electron.* **2019**, *71*, 131–135. [[CrossRef](#)]
19. Ju, H.; Park, D.; Kim, J. Fabrication of porous SnS nanosheets and their combination with conductive polymer for hybrid thermoelectric application. *Chem. Eng. J.* **2019**, *356*, 950–954. [[CrossRef](#)]
20. Ju, H.; Park, D.; Kim, J. Conductive polymer based high-performance hybrid thermoelectrics: Polyaniline/tin (II) sulfide nanosheet composites. *Polymer* **2019**, *160*, 24–29. [[CrossRef](#)]
21. Ju, H.; Kim, M.; Kim, J. Enhanced thermoelectric performance of highly conductive poly (3, 4-ethylenedioxythiophene)/carbon black nanocomposites for energy harvesting. *Microelectron. Eng.* **2015**, *136*, 8–14. [[CrossRef](#)]
22. Wang, Y.; Yang, J.; Wang, L.; Du, K.; Yin, Q.; Yin, Q.J. Polypyrrole/graphene/polyaniline ternary nanocomposite with high thermoelectric power factor. *ACS Appl. Mater. Interfaces* **2017**, *9*, 20124–20131. [[CrossRef](#)] [[PubMed](#)]
23. Shi, H.; Liu, C.; Xu, J.; Song, H.; Lu, B.; Jiang, F.; Zhou, W.; Zhang, G.; Jiang, Q. Facile fabrication of PEDOT: PSS/polythiophenes bilayered nanofilms on pure organic electrodes and their thermoelectric performance. *ACS Appl. Mater. Interfaces* **2013**, *5*, 12811–12819. [[CrossRef](#)] [[PubMed](#)]
24. Ju, H.; Kim, J. Chemically exfoliated SnSe nanosheets and their SnSe/poly (3, 4-ethylenedioxythiophene): Poly (styrenesulfonate) composite films for polymer based thermoelectric applications. *ACS Nano* **2016**, *10*, 5730–5739. [[CrossRef](#)]
25. Mitra, M.; Kargupta, K.; Ganguly, S.; Goswami, S.; Banerjee, D. Facile synthesis and thermoelectric properties of aluminum doped zinc oxide/polyaniline (AZO/PANI) hybrid. *Synth. Met.* **2017**, *228*, 25–31. [[CrossRef](#)]
26. Mitra, M.; Kulsi, C.; Kargupta, K.; Ganguly, S.; Banerjee, D. Composite of polyaniline-bismuth selenide with enhanced thermoelectric performance. *J. Appl. Polym. Sci.* **2018**, *135*, 46887. [[CrossRef](#)]
27. Chatterjee, M.J.; Banerjee, D.; Chatterjee, K. Composite of single walled carbon nanotube and sulfosalicylic acid doped polyaniline: A thermoelectric material. *Mater. Res. Express* **2016**, *3*, 085009. [[CrossRef](#)]
28. Wang, W.; Zhang, Q.; Li, J.; Liu, X.; Wang, L.; Zhu, J.; Luo, W.; Jiang, W. An efficient thermoelectric material: Preparation of reduced graphene oxide/polyaniline hybrid composites by cryogenic grinding. *RSC Adv.* **2015**, *5*, 8988–8995. [[CrossRef](#)]
29. Anno, H.; Hokazono, M.; Akagi, F.; Hojo, M.; Toshima, N. Thermoelectric properties of polyaniline films with different doping concentrations of (±)-10-camphorsulfonic acid. *J. Electron. Mater.* **2013**, *42*, 1346–1351. [[CrossRef](#)]
30. Wang, Y.; Zhang, S.; Deng, Y. Flexible low-grade energy utilization devices based on high-performance thermoelectric polyaniline/tellurium nanorod hybrid films. *J. Mater. Chem. A* **2016**, *4*, 3554–3559. [[CrossRef](#)]
31. Liu, D.; Zhang, Y.; Kang, H.; Li, J.; Chen, Z.; Wang, T. Direct preparation of La-doped SrTiO<sub>3</sub> thermoelectric materials by mechanical alloying with carbon burial sintering. *J. Eur. Ceram. Soc.* **2018**, *38*, 807–811. [[CrossRef](#)]

32. Ju, H.; Kim, J. Preparation and structure dependent thermoelectric properties of nanostructured bulk bismuth telluride with graphene. *J. Alloys Compd.* **2016**, *664*, 639–647. [[CrossRef](#)]
33. Park, D.; Ju, H.; Kim, J. Enhanced thermoelectric power factor and low thermal conductivity in one-dimensional Te/Ag<sub>2</sub>Te composites. *Ceram. Int.* **2017**, *43*, 11156–11162. [[CrossRef](#)]
34. Chen, J.; Sun, T.; Sim, D.; Peng, H.; Wang, H.; Fan, S.; Hng, H.H.; Ma, J.; Boey, F.Y.C.; Li, S. Sb<sub>2</sub>Te<sub>3</sub> nanoparticles with enhanced Seebeck coefficient and low thermal conductivity. *Chem. Mater.* **2010**, *22*, 3086–3092. [[CrossRef](#)]
35. Zhang, Q.; Huang, Y.; Xu, L.; Cao, J.-J.; Ho, W.; Lee, S.C. Visible-light-active plasmonic Ag–SrTiO<sub>3</sub> nanocomposites for the degradation of NO in air with high selectivity. *ACS Appl. Mater. Interfaces* **2016**, *8*, 4165–4174. [[CrossRef](#)] [[PubMed](#)]
36. Sharma, D.; Upadhyay, S.; Satsangi, V.R.; Shrivastav, R.; Waghmare, U.V.; Dass, S. Improved photoelectrochemical water splitting performance of Cu<sub>2</sub>O/SrTiO<sub>3</sub> heterojunction photoelectrode. *J. Phys. Chem. C* **2014**, *118*, 25320–25329. [[CrossRef](#)]
37. Xing, G.; Zhao, L.; Sun, T.; Su, Y.; Wang, X. Hydrothermal derived nitrogen doped SrTiO<sub>3</sub> for efficient visible light driven photocatalytic reduction of chromium (VI). *SpringerPlus* **2016**, *5*, 1132. [[CrossRef](#)]
38. Dong, Y.; Zhou, Y.; Ding, Y.; Chu, X.; Wang, C. Sensitive detection of Pb (II) at gold nanoparticle/polyaniline/graphene modified electrode using differential pulse anodic stripping voltammetry. *Anal. Methods* **2014**, *6*, 9367–9374. [[CrossRef](#)]
39. Kumar, V.; Yokozeki, T.; Goto, T.; Takahashi, T. Synthesis and characterization of PANI-DBSA/DVB composite using roll-milled PANI-DBSA complex. *Polymer* **2016**, *86*, 129–137. [[CrossRef](#)]
40. Wang, N.; He, H.; Li, X.; Han, L.; Zhang, C. Enhanced thermoelectric properties of Nb-doped SrTiO<sub>3</sub> polycrystalline ceramic by titanate nanotube addition. *J. Alloys Compd.* **2010**, *506*, 293–296. [[CrossRef](#)]
41. Shin, H.S.; Jeon, S.G.; Yu, J.; Kim, Y.-S.; Park, H.M.; Song, J.Y. Twin-driven thermoelectric figure-of-merit enhancement of Bi<sub>2</sub>Te<sub>3</sub> nanowires. *Nanoscale* **2014**, *6*, 6158–6165. [[CrossRef](#)] [[PubMed](#)]
42. Kim, G.H.; Hwang, D.H.; Woo, S.I. Thermoelectric properties of nanocomposite thin films prepared with poly (3, 4-ethylenedioxythiophene) poly (styrenesulfonate) and graphene. *Phys. Chem. Chem. Phys.* **2012**, *14*, 3530–3536. [[CrossRef](#)] [[PubMed](#)]



© 2020 by the authors. Licensee MDPI, Basel, Switzerland. This article is an open access article distributed under the terms and conditions of the Creative Commons Attribution (CC BY) license (<http://creativecommons.org/licenses/by/4.0/>).